



HAL
open science

Continuous Symmetries and Observability Properties in Autonomous Navigation

Agostino Martinelli

► **To cite this version:**

Agostino Martinelli. Continuous Symmetries and Observability Properties in Autonomous Navigation. [Research Report] RR-7049, 2009. inria-00421233v1

HAL Id: inria-00421233

<https://inria.hal.science/inria-00421233v1>

Submitted on 1 Oct 2009 (v1), last revised 17 Oct 2010 (v3)

HAL is a multi-disciplinary open access archive for the deposit and dissemination of scientific research documents, whether they are published or not. The documents may come from teaching and research institutions in France or abroad, or from public or private research centers.

L'archive ouverte pluridisciplinaire **HAL**, est destinée au dépôt et à la diffusion de documents scientifiques de niveau recherche, publiés ou non, émanant des établissements d'enseignement et de recherche français ou étrangers, des laboratoires publics ou privés.



INSTITUT NATIONAL DE RECHERCHE EN INFORMATIQUE ET EN AUTOMATIQUE

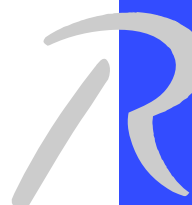
*Continuous Symmetries and Observability Properties
in Autonomous Navigation*

Agostino Martinelli

N° 7049

Octobre 2009

Thèmes COG et NUM



*R*apport
de recherche

Continuous Symmetries and Observability Properties in Autonomous Navigation

Agostino Martinelli

Thèmes COG et NUM — Systèmes cognitifs et Systèmes numériques
Équipe-Projet Emotion

Rapport de recherche n° 7049 — Octobre 2009 — 36 pages

Abstract: This paper considers the problem of estimation in autonomous navigation from a theoretical perspective. In particular, the investigation regards problems where the information provided by the sensor data is not sufficient to carry out the state estimation (i.e. the state is not observable). For these systems, it is introduced the concept of continuous symmetry. Detecting the continuous symmetries of a given system has a very practical importance. It allows us to detect an observable state whose components are non linear functions of the original non observable state. In order to illustrate the power of this concept, its application to a fundamental calibration problem is here presented. This paper provides two distinct contributions. The first one is the introduction in the frame work of autonomous navigation of this concept of continuous symmetry. The second one is the introduction of a simple and efficient strategy to extrinsically calibrate a bearing sensor (e.g. a vision sensor) mounted on a vehicle and simultaneously estimate the parameters describing the systematic error of its odometry system. The strategy uses a single point feature. Many accurate simulations and real experiments with the robot e-Puck equipped with encoder sensors and a camera show the robustness the efficiency and the accuracy of the proposed strategy.

Key-words: State Estimation and Navigation, Sensor Fusion, Localization, Non Observability, Calibration, Mobile Robotics

Symétries Continues et Propriétés d'Observabilité dans la Navigation Autonome

Résumé : Ce document considère le problème de l'estimation en robotique mobile depuis un point de vue théorique. Plus précisément on considère situations où l'information contenue dans les données des capteurs est pas suffisante pour l'estimation (c'est-à-dire l'état n'est pas observable). Pour ces systèmes on introduit le concept de symétrie continue. Détecter les symétries continues d'un tel système est très importante en pratique. Il permet de trouver un nouvel état observable dont les composantes sont fonctions non linéaires de l'état originel. Pour montrer la puissance de ce concept son application à un problème d'auto calibration sera présenté. Ce document contient deux contributions. La première est l'introduction de ce concept de symétrie continue. La deuxième est une technique très efficace et performante pour calibrer les paramètres extrinsèques d'un capteur capable de donner les angles de vue d'une caméra (une camera) et au même temps les paramètres qui donnent la calibration d'un système odomètre. Ce document contient aussi une validation de la technique soit avec des simulations soit avec expérimentations réelles avec le robot mobile e-puck.

Mots-clés : Estimation et Navigation, Fusion Sensorielle, Localisation, Non observabilité, Calibration, Robots Mobiles

1 Introduction

Autonomous navigation requires in many cases to solve simultaneously different tasks (e.g. localization, mapping, obstacle avoidance etc.). Among them, several are estimation tasks, i.e. the robot has to be able to autonomously estimate a given state by integrating the information contained in its sensor data. Typical examples of estimation problems fundamental in many robotics applications are localization, SLAM and self-calibration. In all these problems the goal is to estimate a given state starting from the sensor data.

In every estimation problem the following fundamental questions must be answered:

1. Does the system contain the necessary information to perform the estimation of the considered state?
2. In the case the answer to the previous question is negative, is it possible to detect a new state for which the information allows performing the estimation? And more importantly: what is the link between this new state and the data provided by the robot's sensors?

The answer to the first question is provided by a well known concept developed in the framework of control theory: the observability. In control theory, a system is defined observable when it is possible to reconstruct its initial state by knowing, in a given time interval, the control inputs and the outputs [6]. In mobile robotics the control inputs are usually evaluated by the robot proprioceptive sensors and the outputs by the exteroceptive sensors. The observability properties can be easily derived in a linear system by performing the so called Kalman canonical decomposition (see, e.g., [6]). However, in a non linear system, this concept is much more complex and the observability becomes a local property [13]. In a nonlinear system the concept of *Weak Local Observability* was introduced by Hermann and Krener [11]. The same authors introduced also a criterion, the *observability rank criterion*, to verify whether a system has this property. In particular, the two theorems 3.1 and 3.11 in [11] state that a system is *Weak Local Observable (WLO)* if and only if it satisfies the rank criterion. The application of the rank criterion only requires to perform differentiation. In this paper we make the assumption that a system contains the information to perform the estimation of the state if and only if the system is *WLO*. Obviously, in order to estimate a state it is necessary that the system is *WLO*. However, the contrary cannot be true in some special situations. For instance, this assumption does not take into account the sensor noise. Furthermore, it can be wrong for the kidnapping problem. However, we believe that this assumption is true in many estimation problems in the frame work of autonomous navigation. On the other hand, this assumption has already been adopted in previous works which investigate several estimation problems in the context of mobile robotics (see section 1.2). This assumption allows us to give an answer to the first question by simply performing differentiation.

Answering the second question is in general much harder and can be done by using the theory of distributions [13]. When a system is not *WLO* there are in general infinite possible initial states reproducing exactly the same inputs and outputs. Let us consider for instance the *2D-SLAM* problem when the robot is equipped with odometry sensors and sensors able to perform relative

observations (e.g. bearing and range sensors). We remark that the robot is not equipped with sensors able to perform absolute observations (e.g. GPS and/or compass). Under these hypotheses, all the initial states differing for a shift and a rotation reproduce exactly the same inputs and outputs. Intuitively, we remark that the entire system has three continuous symmetries corresponding to the shift and the rotation on a $2D$ space. Furthermore, it is obvious that the only quantities that we can estimate (i.e. that are *WLO*) satisfy all these three symmetries. The previous consideration regarding the case of $2D$ -SLAM is pretty trivial and does not require to introduce special mathematical tools (e.g. the theory of distributions) in order to achieve practical results. However, there are cases where it is a very challenging task answering the second question, i.e. detecting a new *WLO* state and its link with the data provided by the robot's sensors.

In the theory of distributions introduced in [13] the concept of continuous symmetry is implicitly contained in the Frobenius theorem through the Lie brackets. In this paper we provide first of all a definition of continuous symmetry and, starting from it, we derive a partial differential equation which must be satisfied by all the *WLO* quantities. The same partial differential equation is derived in [13]. However, the derivation here provided is much simpler since does not require to introduce the Lie brackets, the Frobenius theorem and the concept of distribution. Therefore, we believe that it can be very useful for the mobile robotics community. We then consider a fundamental calibration problem: the simultaneous self calibration of the odometry system and the extrinsic calibration of a bearing sensor. In particular, we consider the case when the calibration is carried out by only using a single point feature. To the best of our knowledge this problem has never been investigated before. Contrary to the $2D$ -SLAM previously mentioned, it is impossible to derive for this problem the *WLO* quantities without performing analytical computation. In particular, we provide the steps to solve this calibration problem on the basis of the analytical results derived in the first part of this paper.

1.1 Related Works on Sensor Calibration in Mobile Robotics

In the last decades, the problem of sensor calibration has been considered with special emphasis in the field of computer vision. In robotics, when a camera is adopted, the calibration only regards the estimation of the extrinsic parameters, i.e. the parameters describing the configuration of the camera in the robot frame. In the case of robot wrists, very successful approaches are based on the solution of a homogeneous transform equation of the form $AX = XB$ which is obtained by moving the robot wrist and observing the resulting motion of the camera [26, 29]. In particular, in the previous equation, A describes the configuration change of the wrist, B the configuration change of the camera and X the unknown camera configuration in the wrist reference frame. A and B are assumed to be known with high accuracy: A is obtained by using the encoder data and B by using the camera observations of a known object before and after the wrist movement [29]. In mobile robotics the situation changes dramatically and the previous methods cannot be applied. Unfortunately, the displacement of a mobile robot obtained by using the encoder data is not precise as in the case of a wrist. In other words, the previous matrix A is roughly estimated by the encoders. A possible solution to this inconvenient could be obtained by

adopting other sensors to estimate the robot movement (i.e. the matrix A). However, most of times the objective is to estimate the camera configuration in the reference frame attached to the robot odometry system. Therefore, it is important to introduce a new method able to perform simultaneously the extrinsic camera calibration and the calibration of the robot odometry system. So far, the two problems have been considered separately.

Regarding the odometry, a very successful strategy has been introduced in 1996 by Borenstein and Feng [5]. This is the UMBmark method. It is based on absolute robot position measurements after the execution of several square trajectories. In [17] the problem of also estimating the non-systematic odometry errors was considered. More recently, a method based on two successive least-squares estimations has been introduced [2]. Finally, very few approaches calibrate the odometry without the need of an a priori knowledge of the environment and/or of the use of global position sensors (like a GPS) [9, 28, 30].

Regarding the problem of sensor to sensor calibration, several cases have recently been considered (e.g. IMU-camera [25], laser scanner-camera [7], [31], [32] and odometry-camera [20]).

1.2 Related Works on Observability Analysis in Mobile Robotics

Regarding the localization problem, the observability analysis has been carried out by several authors. Roumeliotis [27] presented it for a multi robots system equipped with encoder and sensors able to provide an observation consisting of the relative configuration between each pair of robots. The analysis was performed through the linear approximation. The main result of this observability analysis was that the system is not observable and it becomes observable when at least one of the robots in the team has global positioning capabilities. Bonifait and Garcia considered the case of one robot equipped with encoders and sensors able to provide the bearing angles of known landmarks in the environment [4]. The observability analysis was carried out by linearizing the system (as in the previous case) and by applying the *observability rank condition*. As in many nonlinear systems, they found that in some cases while the associated linearized system is not observable, the system is *WLO*. These results have been extended to the case of two robots in [19]. Furthermore, Bicchi and collaborators extended the case of a single robot to the SLAM problem ([3], [16]). They considered one robot equipped with the same bearing sensors of the previous case. They considered in the environment landmarks with a priori known position and landmarks whose position has to be estimated. They found that two landmarks are necessary and sufficient to make the system observable. Furthermore, they applied optimal control methods in order to minimize the estimation error. In particular, in [16] they maximized the Cramer-Rao lower bound as defined in [14]. Very recently, the observability rank condition has been adopted to investigate the observability properties for the problem of simultaneously localizing a mobile robot and calibrating its odometry system [21]. Also the case of a vision sensor has been considered [20] [25]. Finally, the observability rank criterion has recently been applied to the SLAM problem [12] [15].

However, in all these works what it was determined is only whether the state defining the system configuration is *WLO* or not.

1.3 Paper Contributions and Paper Structure

In this paper we want to do a step forward whose importance is in our opinion fundamental when dealing with a non observable problem. Indeed, when a state is not *WLO*, estimating directly the state brings to inconsistency with catastrophic consequences. On the other hand, when a state is not *WLO*, suitable functions of its components could be *WLO* and therefore could be estimated. The derivation of these functions and their link with the data provided by the robot's sensors is fundamental in order to properly perform the estimation.

This paper provides two distinct contributions:

- The introduction in the frame work of autonomous navigation of some mathematical tools taken from control theory to derive the *WLO* quantities for robotics systems which are not *WLO* and their link with the data provided by the robot's sensors;
- The use of these tools to introduce a new strategy to robustly, efficiently and accurately estimate the parameters describing both the extrinsic bearing sensor calibration and the odometry calibration.

The second contribution was preliminary discussed in [23] and [24] where the same calibration problem has been analyzed. In particular, in [23] it was performed a local decomposition for this system when the robot accomplishes pure rotations and straight paths. In [24] the local decomposition was extended to any circular trajectory.

Section 2 provides a very simple example to better illustrate the first contribution of this paper. As for the previously considered *2D*-SLAM, analytical methods are not required to detect the *WLO* quantities due to the simplicity of the chosen example. The theoretical concepts introduced in section 3 will be illustrated by referring to this simple example. In particular, we remind the rank criterion introduced by Hermann and Krener [11] and we introduce the concept of continuous symmetry. Starting from this definition we derive a partial differential equation which characterizes all the *WLO* quantities in a given system. In section 4 we derive these *WLO* quantities for our calibration problem. Starting from the decomposition given in section 4 we introduce a very efficient strategy to perform the calibration in section 5. Finally, we evaluate its performance in section 6, with simulations (6.1) and real experiments (6.2). Conclusions are provided in section 7.

2 A Simple Example of Localization

We consider a mobile robot moving in a *2D*-environment. The configuration of the robot in a global reference frame can be characterized through the vector $[x_R, y_R, \theta_R]^T$ where x_R and y_R are the cartesian robot coordinates and θ_R is the robot orientation. The dynamics of this vector are described by the following non-linear differential equations:

$$\begin{cases} \dot{x}_R = v \cos \theta_R \\ \dot{y}_R = v \sin \theta_R \\ \dot{\theta}_R = \omega \end{cases} \quad (1)$$

where v and ω are the linear and the rotational robot speed, respectively. The robot is equipped with proprioceptive sensors able to evaluate these two speeds. We assume that it exists a point feature in our environment and, without loss of generality, we fix the global reference frame on it (see figure 1a). The robot is also equipped with a range sensor able to evaluate the distance of the point feature. Therefore, our system has the following output:

$$y = D \equiv \sqrt{x_R^2 + y_R^2} \quad (2)$$

We also provide the equations for the same system in polar coordinates, i.e. when the robot configuration is described by the coordinates D , $\phi_R \equiv \text{atan2}(y_R, x_R)$ and θ_R .

$$\begin{cases} \dot{D} = v \cos(\theta_R - \phi_R) \\ \dot{\phi}_R = \frac{v}{D} \sin(\theta_R - \phi_R) \\ \dot{\theta}_R = \omega \\ y = D \end{cases} \quad (3)$$

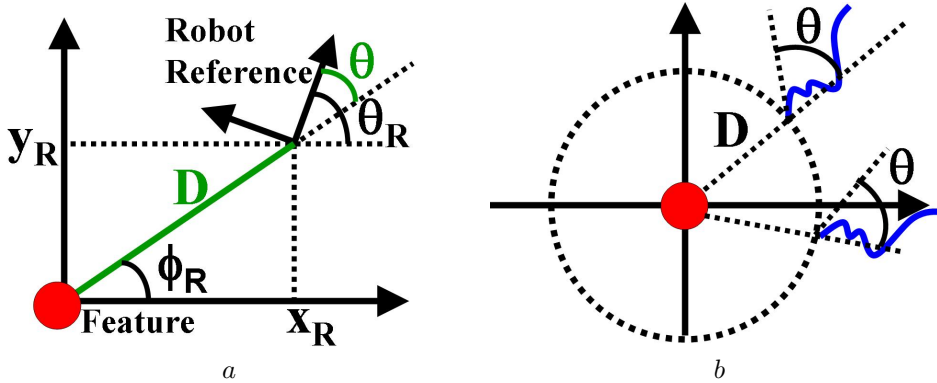


Figure 1: A simple localization problem. The robot is equipped with odometry sensors and range sensors able to evaluate the distance D (a). In b the two trajectories are compatible with the same system inputs and outputs.

Our goal is to answer the two questions mentioned in the previous section for the system characterized by the equations (1-2) or (3). Since the system is very simple, we do not need special mathematical tools.

To check whether we have the necessary information to estimate the robot configuration $[x_R, y_R, \theta_R]^T$ we have to prove that it is possible to uniquely reconstruct the initial robot configuration by knowing the input controls and the outputs (observations) in a given time interval. When at the initial time the distance D from the origin is available, the estimated robot position belongs to a circumference (see figure 1b). Furthermore, every orientation is possible. As soon as the robot moves accordingly to the inputs $v(t)$ and $\omega(t)$, it is possible to find one trajectory starting from each point on the circumference providing the same distances from the origin by choosing a suitable initial robot orientation (e.g. in fig. 1b the two indicated trajectories provide the same distances from

the origin at every time). Therefore, the dimension of the undistinguishable region is 1 and the dimension of the largest *WLO* subsystem is $3 - 1 = 2$.

We remark that the system has a continuous symmetry: the system inputs ($v(t)$ and $\omega(t)$) and outputs ($y(t)$) are invariant with respect to a rotation of the global frame about the vertical axis (in the next section we will provide a mathematical definition for a general continuous symmetry). From the fact that the dimension of the largest *WLO* subsystem is two, we know that we can only estimate two independent quantities. Furthermore, these two quantities must satisfy the previous system invariance, i.e. they must be rotation invariant. A possible choice is provided by the two quantities D and θ in figure 1.

$$\theta \equiv \theta_R - \text{atan2}(y_R, x_R) \quad (4)$$

The new system is characterized by the following equations:

$$\begin{cases} \dot{D} = v \cos \theta \\ \dot{\theta} = \omega - \frac{v}{D} \sin \theta \\ y = D \end{cases} \quad (5)$$

which express the link between the new state $[D, \theta]^T$ and the proprioceptive data (v, ω) and the exteroceptive data (D).

The detection of the previous two quantities and the derivation of the equations in (5) is fundamental (i.e the answer to the second question stated in the introduction). Indeed, estimating the original state brings to inconsistency with catastrophic consequences.

In the next section we want to provide some mathematical tools (taken from control theory) in order to perform the same analysis. This will allow us to answer the two questions stated in the introduction for more complicated estimation problems in the frame work of autonomous navigation.

3 Continuous Symmetries and Observability Properties

A general characterization for systems in the frame work of autonomous navigation is provided by the following equations:

$$\begin{cases} \dot{S} = \sum_{i=1}^M f_i(S)u_i \\ y = h(S) \end{cases} \quad (6)$$

where $S \in \Sigma \subseteq \mathfrak{R}^n$ is the state, u_i are the system inputs, $y \in \mathfrak{R}$ is the output (we are considering a scalar output for the sake of clarity, the extension to a multi dimensions output is straightforward). In control theory it is very common to add a term $f_0(S)$ in the first equation in (6), i.e. independent of the system inputs. Both the systems defined by (1-2) or (3) and the one defined by (5) can be characterized by (6). For instance, for the system in (3) we have: $S = [D, \phi_R, \theta_R]^T$, $M = 2$, $u_1 = v$, $u_2 = \omega$, $f_1(S) = [\cos(\theta_R - \phi_R), \frac{\sin(\theta_R - \phi_R)}{D}, 0]^T$, $f_2(S) = [0, 0, 1]^T$, $h(S) = D$.

3.1 Observability Rank Criterion

We want to remind some concepts in the theory by Hermann and Krener in [11]. We will adopt the following notation. We indicate the k^{th} order Lie derivative of a field Λ along the vector fields $v_{i_1}, v_{i_2}, \dots, v_{i_k}$ with $L_{v_{i_1}, v_{i_2}, \dots, v_{i_k}}^k \Lambda$. We remind the definition of the Lie derivative. It is provided by the following two equations:

$$L^0 \Lambda = \Lambda, \quad (7)$$

$$L_{v_{i_1}, \dots, v_{i_k}, v_{i_{k+1}}}^{k+1} \Lambda = \nabla_S \left(L_{v_{i_1}, \dots, v_{i_k}}^k \Lambda \right) \cdot v_{i_{k+1}}$$

where the symbol " \cdot " denotes the scalar product. Now, let us refer to the system in (6) and let us indicate with Ω the space of all the Lie derivatives $L_{f_{i_1}, \dots, f_{i_k}}^k h$, ($i_1, \dots, i_k = 1, \dots, M$) and the functions f_{i_j} ($j = (1, \dots, M)$) are defined in (6). Furthermore, we denote with $dL_{f_{i_1}, \dots, f_{i_k}}^k h$ the gradient of the corresponding Lie derivative (i.e. $dL_{f_{i_1}, \dots, f_{i_k}}^k h \equiv \nabla_S L_{f_{i_1}, \dots, f_{i_k}}^k h$) and we denote with $d\Omega$ the space spanned by all these gradients.

In this notation, the observability rank criterion can be expressed in the following way: *The dimension of the largest WLO sub-system at a given S_0 is equal to the dimension of $d\Omega$.*

We now consider again the simple example introduced in section 2 and we show that by using the observability rank criterion we can answer the first question stated in the introduction. In particular, we obtain the same answer already provided in section 2.

The computation of the rank for the system in (3) is straightforward. From the last equation in (3) we obtain: $L^0 h = D$ whose gradient is $dL^0 h \equiv w_1 = [1, 0, 0]$. The first order Lie derivatives are: $L_{f_1}^1 h = \cos(\theta_R - \phi_R)$ and $L_{f_2}^1 h = 0$. We have: $dL_{f_1}^1 h \equiv w_2 = [0, \sin(\theta_R - \phi_R), -\sin(\theta_R - \phi_R)]$. It is easy to realize that each vector w_i obtained by extending the previous computation to every Lie derivative order has the structure: $w_i = [\rho_i, \varsigma_i, -\varsigma_i]$. Indeed, every Lie derivative will depend on θ_R and ϕ_R only through the quantity $\theta_R - \phi_R$, which changes in sign with respect to the change $\theta_R \leftrightarrow \phi_R$. Therefore, the rank of the matrix

$$\Gamma \equiv \left\{ \begin{array}{c} w_1 \\ w_2 \\ \dots \\ w_i \\ \dots \end{array} \right\} \quad (8)$$

is equal to two. We conclude that the largest WLO sub-system has dimension two as derived in section 2.

3.2 Local Decomposition

Let us suppose that the system in (6) is not WLO and that the dimension of the largest WLO subsystem is n_{obs} . According to the theory of distributions developed in [13], we can find n_{obs} independent functions of the components of the original state S which are WLO and $n - n_{obs}$ independent functions of the components of S which are not WLO. More precisely, if we include the n_{obs}

WLO functions in the vector S_b and the other $n - n_{obs}$ functions in the vector S_a , we have the following decomposition for the original system:

$$\begin{cases} \dot{S}_a = \sum_{i=1}^M f_i^a(S_a, S_b)u_i \\ \dot{S}_b = \sum_{i=1}^M f_i^b(S_b)u_i \\ y = h_b(S_b) \end{cases} \quad (9)$$

In particular, the subsystem defined by the last two equations in (9) is independent of the value of S_a and it is WLO . Therefore, by performing this decomposition, we can use the information coming from the dynamics (i.e. the knowledge of $u(t)$) and the observations ($y(t)$) in order to estimate the WLO quantities (S_b). This decomposition extends the Kalman canonical decomposition to the non linear case. It is fundamental in every estimation problem when the state is not observable. Indeed, estimating directly the original state S results in an erroneous evaluation.

In section 2 the equations in (5) represent such a decomposition for the system defined by (1-2) or (3).

3.3 Continuous Symmetries

In this subsection we provide a simple derivation of a result available in the first chapter of [13]. In that chapter, the concept of continuous symmetry is not explicitly mentioned. However, it is implicitly contained in the Frobenius theorem through the Lie brackets. This result can significantly help in order to perform the decomposition given in 3.2 for real systems in mobile robotics as will be shown in the next sections.

We introduce the following definition:

Definition 1 (Continuous Symmetry) *The vector field $w_s(S)$ ($S \in \Sigma$) is a continuous symmetry in S for the system defined in (6) if and only if it is a non null vector belonging to the null space of the matrix whose lines are the gradients of all the Lie derivatives computed in S .*

For the system defined by (3) it exists only one continuous symmetry given by the vector $[0, 1, 1]^T$ (i.e. belonging to the null space of the matrix Γ in (8)). We remark that in this case the symmetry is independent of S .

Let us consider a point $S_0 \in \Sigma$ and the curve $S(S_0, \tau)$ in Σ which is the solution of the differential equation:

$$\begin{cases} \frac{dS}{d\tau} = w_s(S) \\ S(0) = S_0 \end{cases} \quad (10)$$

(we assume suitable regularity hypothesis on $w_s(S)$ in order to guarantee the existence of a unique solution).

We have the following property:

Property 1 A scalar and differentiable function $g(S)$ ($S \in \Sigma$) is constant on the curve $S(S_0, \tau)$ if and only if its gradient is orthogonal to $w_s(S)$.

Proof: Proving this property is immediate. We have: $\frac{dg(S(S_0, \tau))}{d\tau} = \nabla_S g \cdot \frac{dS}{d\tau} = \nabla_S g \cdot w_s$.

According to the definition given before, w_s is orthogonal to the gradients of all the Lie derivatives. This means that all the Lie derivatives are constant on the curve $S(S_0, \tau)$. In other words, all the initial conditions belonging to this curve, produce the same Lie derivatives for the system given in (6) at the initial time. On the other hand, the knowledge of all the Lie derivatives at the initial time is equivalent to the knowledge of the system inputs and outputs in the time interval starting from that time. This equivalence is at the basis of the theory introduced by Hermann and Krener in [11] and it is a consequence of the two theorems of the implicit functions and the Taylor expansion.

Therefore, the solution $S(S_0, \tau)$ of (10) provides a set of infinite initial states producing exactly the same system inputs and outputs. In other words, these points are indistinguishable.

The information contained in the system inputs and outputs cannot distinguish the points belonging to the curve $S(S_0, \tau)$. Therefore, these data do not contain the information to estimate a quantity $g(S)$ which is not constant on this curve. This proves the following fundamental property:

Property 2 Given a scalar function $g(S)$ defined in the configuration space of (6), a necessary condition to be WLO is that its gradient is orthogonal to $w_s(S)$ (i.e. $\nabla_S g \cdot w_s(S) = 0$).

This necessary condition can be expressed by the following partial differential equation:

$$\sum_{i=1}^n w_{si}(S) \frac{\partial g}{\partial S_i} = 0 \quad (11)$$

where $w_{si}(S)$ is the i^{th} component of the symmetry w_s . The previous equation must be satisfied by all the WLO quantities. This equation can significantly help to perform the decomposition given in (9) as will be shown in the next sections.

We conclude this section by discussing the previous concepts for the example in section 2.

As previously remarked, in this case we have a single continuous symmetry given by the vector $[0, 1, 1]^T$. Furthermore, a possible description for the curve $S(S_0, \tau)$ is in this case:

$$\begin{cases} D(\tau) = D_0 \\ \phi_R(\tau) = \tau \\ \theta_R(\tau) = \tau + \theta_0 \end{cases}$$

where D_0 and θ_0 depend on S_0 (they are τ independent).

Finally, we use (11) to detect the two WLO quantities. The equation (11) becomes: $\frac{\partial g}{\partial \phi_R} + \frac{\partial g}{\partial \theta_R} = 0$ and two independent solutions are $g = D$ and $g = \theta_R - \phi_R$. This is the same result we obtained in section 2.

4 The Problem of Simultaneous Odometry and Bearing Sensor Calibration

In contrast with the simple example introduced in section 2 where a simple intuitive procedure provides the answers to the theoretical questions stated in the introduction, there are cases where the application of the previous concepts and in particular the use of (11) is required. In this section we will discuss a calibration problem where we make use of these concepts.

4.1 The Considered System

We consider again a mobile robot moving in a $2D$ -environment whose dynamics are described by (1). Now we assume that the odometry sensors do not provide directly v and ω . We will consider the case of a differential drive and, in order to characterize the systematic odometry errors, we adopt the model introduced in [5]. We have:

$$v = \frac{\delta_R v_R + \delta_L v_L}{2} \quad \omega = \frac{\delta_R v_R - \delta_L v_L}{\delta_B B} \quad (12)$$

where v_R and v_L are the control velocities (i.e. $u = [v_R, v_L]^T$) for the right and the left wheel, B is the nominal value for the distance between the robot wheels and δ_R , δ_L and δ_B characterize the systematic odometry error due to an uncertainty on the wheels diameters and on the distance between the wheels.

Furthermore, a bearing sensor (e.g. a camera) is mounted on the robot. We assume that its vertical axis is aligned with the z -axis of the robot reference frame and therefore the transformation between the frame attached to this sensor and the one of the robot is characterized through the three parameters ϕ , ρ and ψ (see fig. 2).

The available data are the control $u = [v_R, v_L]^T$ and the bearing angle of a single feature (β in fig. 2) at several time steps during the robot motion.

We introduce the following quantities:

$$\mu \equiv \frac{\rho}{D}; \quad \gamma \equiv \theta + \phi; \quad (13)$$

By using simple trigonometry algebra we obtain (see also fig. 2):

$$\beta = \begin{cases} -\operatorname{atan}\left(\frac{\sin \gamma}{\mu + \cos \gamma}\right) - \psi + \pi & \text{if } \gamma_- \leq \gamma \leq \gamma_+ \\ -\operatorname{atan}\left(\frac{\sin \gamma}{\mu + \cos \gamma}\right) - \psi & \text{otherwise} \end{cases}$$

where γ_- and γ_+ are the two solutions (in $[-\pi, \pi)$) of the equation $\cos \gamma = -\mu$ with $\gamma_+ = -\gamma_-$ and $\gamma_+ > 0$. We made the assumption $0 < \mu < 1$ since we want to avoid collisions between the robot and the feature ($D > \rho$).

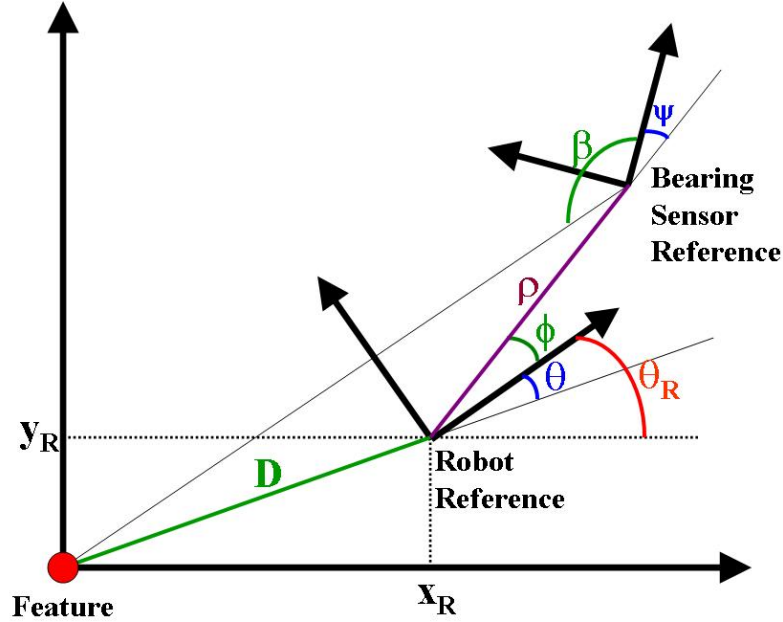


Figure 2: The two reference frames respectively attached to the robot and to the bearing sensor.

By using (1) and the definitions in (13) the dynamics of our system are described by the following equations:

$$\begin{cases} \dot{\mu} = -\mu^2 \frac{v}{\rho} \cos(\gamma - \phi) \\ \dot{\gamma} = \omega - \mu \frac{v}{\rho} \sin(\gamma - \phi) \\ \dot{\phi} = \dot{\rho} = \dot{\psi} = \dot{\delta}_R = \dot{\delta}_L = \dot{\delta}_B = 0 \end{cases} \quad (14)$$

The goal is to simultaneously estimate the parameters ϕ , ρ , ψ , δ_R , δ_L and δ_B by using the available data (i.e. v_R , v_L and β in a given time interval). Since these data consists of angle measurements (the wheel diameters are not known and in fact are to be estimated), the best we can hope is the possibility to estimate these parameters up to a scale factor. In particular, we will refer to the following parameters:

$$\phi, \quad \psi, \quad \eta \equiv \frac{\delta_R}{2\rho}, \quad \delta \equiv \frac{\delta_L}{\delta_R}, \quad \xi \equiv \frac{1}{B} \frac{\delta_R}{\delta_B} \quad (15)$$

Original Calibration Parameters	
Camera: ϕ, ρ, ψ	Odometry: $\delta_R, \delta_L, \delta_B$
Observable Parameters	
$\phi, \psi, \eta \equiv \frac{\delta_R}{2\rho}, \delta \equiv \frac{\delta_L}{\delta_R}, \xi \equiv \frac{1}{B} \frac{\delta_R}{\delta_B}$	
Parameters observable in a single q-trajectory	
$A^q \equiv \frac{\Psi_1^q - \Psi_3}{1 + \Psi_1^q \Psi_3}, V^q \equiv \Psi_2^q \frac{1 + \Psi_1^q \Psi_3}{1 + \Psi_3^2}, L^q \equiv \psi - \text{atan} \Psi_1^q, \xi_q \equiv \xi(1 - q\delta)$	
where: $\Psi_1^q \equiv \frac{\xi_q - \eta_q \sin \phi}{\eta_q \cos \phi}, \Psi_2^q \equiv \frac{\mu \eta_q \cos \phi}{\sin \gamma},$	
$\Psi_3 \equiv \frac{\mu + \cos \gamma}{\sin \gamma}, \eta_q \equiv \eta(1 + q\delta)$	

Table 1: Variables adopted in our calibration problem

The dynamics and the observation of our system are described by the following equations:

$$\begin{cases} \dot{\mu} = -\mu^2 \eta (v_R + \delta v_L) \cos(\gamma - \phi) \\ \dot{\gamma} = \xi (v_R - \delta v_L) - \mu \eta (v_R + \delta v_L) \sin(\gamma - \phi) \\ \dot{\phi} = \dot{\psi} = \dot{\eta} = \dot{\delta} = \dot{\xi} = 0 \\ \beta = \begin{cases} -\text{atan} \left(\frac{\sin \gamma}{\mu + \cos \gamma} \right) - \psi + \pi & \gamma_- \leq \gamma \leq \gamma_+ \\ -\text{atan} \left(\frac{\sin \gamma}{\mu + \cos \gamma} \right) - \psi & \text{otherwise} \end{cases} \end{cases} \quad (16)$$

The state $[\mu, \gamma, \phi, \psi, \eta, \delta, \xi]^T$ is *WLO* as proven in the appendix. In the next subsection we consider circular trajectories. For them, the overall system is not *WLO*. We separate the part of the system which is *WLO* from the rest. Based on this decomposition, in section 5 we introduce a very efficient strategy to estimate these parameters. Finally, by adding a simple metric measurement (e.g. the initial distance between the robot and the feature) the original parameters $\phi, \rho, \psi, \delta_R, \delta_L$ and δ_B can also be estimated.

For the sake of clarity we report all the variables adopted in the considered calibration problem in table 1.

4.2 Deriving the WLO Quantities for Circular Trajectories

We consider the one-degree of freedom motion obtained by setting $v_R = \nu, v_L = q\nu$ (q-trajectory). Let us define:

$$\eta_q \equiv \eta(1 + q\delta) \quad \xi_q \equiv \xi(1 - q\delta) \quad (17)$$

From the dynamics in (16) we obtain the following dynamics:

$$\begin{cases} \dot{\mu} = -\mu^2 \eta_q \nu \cos(\gamma - \phi) \\ \dot{\gamma} = \xi_q \nu - \mu \eta_q \nu \sin(\gamma - \phi) \\ \dot{\eta}_q = \dot{\xi}_q = \dot{\phi} = \dot{\psi} = 0 \end{cases} \quad (18)$$

In the next we provide the steps necessary to perform the local decomposition of the system whose dynamics are given in (18) and whose output is the

observation β given in (16). We proceed in two separate steps. We first consider the following simpler system:

$$\begin{cases} \dot{\mu} = -\mu^2 \eta_q \nu \cos(\gamma - \phi) \\ \dot{\gamma} = \xi_q \nu - \mu \eta_q \nu \sin(\gamma - \phi) \\ \dot{\eta}_q = \dot{\xi}_q = \dot{\phi} = 0 \\ y = \frac{\sin \gamma}{\mu + \cos \gamma} \end{cases} \quad (19)$$

where we removed the variable ψ . By using the matlab symbolic computation it is possible to detect only the following symmetry:

$$w_s = \left[\mu \cos \gamma + 1, \sin \gamma, \frac{\xi_q \sin \phi - \eta_q}{\mu}, 0, \frac{\xi_q \cos \phi}{\eta_q \mu} \right]^T$$

Since this subsystem is defined by a state whose dimension is five, having one symmetry means that we have four independent *WLO* quantities which must satisfy the partial differential equation given in (11) associated to the previous symmetry, i.e.:

$$(\mu \cos \gamma + 1) \frac{\partial \Psi}{\partial \mu} + \sin \gamma \frac{\partial \Psi}{\partial \gamma} + \frac{\xi_q \sin \phi - \eta_q}{\mu} \frac{\partial \Psi}{\partial \eta_q} + \frac{\xi_q \cos \phi}{\eta_q \mu} \frac{\partial \Psi}{\partial \phi} = 0$$

Finding four independent solutions is not difficult since we know that all the Lie derivatives are solutions. However, we need to express the dynamics and the system output through them, as in the decomposition given in (9). Therefore, we cannot use simply the Lie derivatives since their expression is very complicated (with the exception of the zero-order which coincides with the output $\frac{\sin \gamma}{\mu + \cos \gamma}$). On the other hand, a very simple solution for the previous partial differential equation is provided by ξ_q . By using this solution and the output $\frac{\sin \gamma}{\mu + \cos \gamma}$, and starting from the expressions of the first and second order Lie derivatives, we were able to detect two other solutions: $\frac{\xi_q - \eta_q \sin \phi}{\eta_q \cos \phi}$ and $\frac{\mu \eta_q \cos \phi}{\sin \gamma}$. We therefore find the following four independent *WLO* quantities:

$$\begin{aligned} \Psi_1^q &\equiv \frac{\xi_q - \eta_q \sin \phi}{\eta_q \cos \phi}, & \Psi_2^q &\equiv \frac{\mu \eta_q \cos \phi}{\sin \gamma}, \\ \Psi_3 &\equiv \frac{\mu + \cos \gamma}{\sin \gamma}, & \xi_q & \end{aligned} \quad (20)$$

and the local decomposition of (19) is:

$$\begin{cases} \dot{\Psi}_1^q = 0 \\ \dot{\Psi}_2^q = \nu \Psi_2^q (\Psi_1^q \Psi_2^q - \xi_q \Psi_3) \\ \dot{\Psi}_3 = \nu (\Psi_2^q + \Psi_1^q \Psi_2^q \Psi_3 - \xi_q - \xi_q \Psi_3^2) \\ \dot{\xi}_q = 0 \\ y = \frac{1}{\Psi_3} \end{cases} \quad (21)$$

Let us proceed with the second step. We add to the system in (21) the parameter ψ (with $\dot{\psi} = 0$) and we consider the output $y = \beta = \text{atan}\left(\frac{1}{\Psi_3}\right) - \psi$ instead of $y = \frac{1}{\Psi_3}$.

By using the matlab symbolic computation it is possible to detect again a single symmetry for the resulting system:

$$w_s = \left[\Psi_1^{q^2} + 1, \Psi_2^q(\Psi_3 - \Psi_1^q), \Psi_3^2 + 1, 0, 1, \right]^T$$

The associated partial differential equation is in this case:

$$(\Psi_1^{q^2} + 1) \frac{\partial G}{\partial \Psi_1^q} + (\Psi_2^q(\Psi_3 - \Psi_1^q)) \frac{\partial G}{\partial \Psi_2^q} + (\Psi_3^2 + 1) \frac{\partial G}{\partial \Psi_3} + \frac{\partial G}{\partial \psi} = 0$$

namely, every solution $G(\Psi_1^q, \Psi_2^q, \Psi_3, \xi_q, \psi)$ of the previous partial differential equation is a *WLO* quantity for this resulting system. Again, a very simple solution is provided by ξ_q . Then, by proceeding as before we found the following four independent solutions:

$$\begin{aligned} A^q &\equiv \frac{\Psi_1^q - \Psi_3}{1 + \Psi_1^q \Psi_3}, & V^q &\equiv \Psi_2^q \frac{1 + \Psi_1^q \Psi_3}{1 + \Psi_3^2}, \\ L^q &\equiv \psi - \text{atan} \Psi_1^q, & \xi_q & \end{aligned} \quad (22)$$

and the local decomposition is:

$$\begin{cases} \dot{A}^q = \nu(1 + A^{q^2})(\xi_q - V^q) \\ \dot{V}^q = \nu A^q V^q (2V^q - \xi_q) \\ \dot{L}^q = \dot{\xi}_q = 0 \\ \beta = -\text{atan} A^q - L^q + S_p \frac{\pi}{2} \end{cases} \quad (23)$$

where S_p can be ± 1 depending on the values of the system parameters. We do not provide here this dependence. In [18] we derive some important properties relating S_p to the robot motion.

This decomposition has a very practical importance. It tells us that, when the robot accomplishes circular trajectories, the information contained in the sensor data (i.e. the information contained in the function $\nu(t)$ and $\beta(t)$) allows us to estimate only the state $[A^q, V^q, L^q, \xi_q]^T$ and not the original state $[\mu, \gamma, \phi, \psi, \xi, \delta, \eta]^T$. Furthermore, it provides the link between the observable state $[A^q, V^q, L^q, \xi_q]^T$ and the sensor data ν and β .

4.3 Analytical Properties of the Observation Function

In this section we summarize some important properties of the observation β obtained when the robot accomplishes circular trajectories. These properties are fundamental to introduce our calibration strategy. For the sake of conciseness, we cannot derive these properties here. However, a detailed derivation is available in [18]. Furthermore, it is possible to directly verify the validity of these properties with a simple substitution. For the sake of simplicity in the

next we neglect the suffix q on the three parameters A , V and L . On the other hand, to distinguish ξ_q from ξ previously defined, we still maintain q in ξ_q .

First of all, it is possible to directly integrate the dynamics in (23) to get an analytical expression for β vs the time or vs the curve length s defined by the following equation:

$$s = s(t) = \int_0^t \nu(\tau) d\tau \quad (24)$$

The expression of β vs s is given by the following equations:

$$w = \xi_q \tan(c + S_w \xi_q s) \quad (25)$$

$$V = \frac{\xi_q k(2k - \xi_q) + kw^2 + S_V w \sqrt{k(k - \xi_q)(w^2 + \xi_q^2)}}{(2k - \xi_q)^2 + w^2} \quad (26)$$

$$A = S_y \sqrt{\frac{k(2V - \xi_q) - V^2}{V^2}} \quad (27)$$

$$\beta = \text{atan}(A) - L + S_p \frac{\pi}{2} \quad (28)$$

where S_w , S_V , and S_y are three sign variables, namely, as for S_p , they can assume the value of $+1$ or -1 . c and k are two time-independent parameters whose value depends on the initial robot configuration with respect to the feature. In particular:

$$k = \frac{(1 + A_0^2)V_0^2}{2V_0 - \xi_q} \quad (29)$$

and

$$c = \text{atan} \left(\frac{\xi_q k + (\xi_q - 2k)V_0}{\xi_q \sqrt{-V_0^2 + 2kV_0 - \xi_q k}} \right) \quad (30)$$

The validity of the previous expression for β can be checked by directly computing the time derivatives of V and A respectively in (26) and (27) and by verifying that they satisfy (23).

The variables S_V , S_y and S_p flip in correspondence of special points whose value can be determined by imposing the continuity of the expressions (25-28) and their first derivatives (see [18] for a detailed discussion of this continuity analysis). Among these points, there are the ones where the function w in (25) diverges. We call them nodes. They are:

$$s_n = -S_w \frac{c}{\xi_q} + j \frac{\pi}{\xi_q} + S_w \frac{\pi}{2\xi_q} \quad (31)$$

j being an integer. In other words, there are infinite nodes at the distance of $\frac{\pi}{|\xi_q|}$ one each other.

For every point s we introduce an operation which associates to s the point \hat{s} defined by the following equation:

$$\hat{s} \equiv 2s_n^R - s \quad (32)$$

where s_n^R is the closest node to s on the right. In [18] we derive the following fundamental theorem whose validity can in any case be checked by a direct substitution:

Theorem 1 (Reflection of the Observation Function) *The observation function satisfies the following fundamental equation $\forall s$:*

$$\beta(s) + \beta(\hat{s}) = -2L \pmod{\pi} \quad (33)$$

This theorem is fundamental for estimating the parameters ξ_q , L , k and c related to a given trajectory (see the algorithm 1 in the next section). The name reflection comes from the fact that according to (32) \hat{s} is the reflection of s with respect to the node between them (s_n^R).

The previous theorem is basically a consequence of the circular trajectory accomplished by the robot. However, in [18] its proof is carried out by only performing a continuity analysis on the observation function. The advantage of this analysis is that it provides the behavior of the sign variables (S_V , S_y and S_p).

5 The Strategy to Estimate the System Parameters

It is possible to verify that the observation function is a periodic function whose period is:

$$T_S = \frac{2\pi}{|\xi_q|} \quad (34)$$

Equation (34) allows us to estimate the parameter ξ_q by evaluating the period of the observation function. Actually, this equation does not provide the sign of ξ_q . However, this sign is positive for all the values of $q < \frac{1}{\delta}$ (i.e. when the robot accomplishes counter clock-wise circular trajectories).

Once ξ_q is estimated, the next step consists in the evaluation of the position of one node. Indeed, once we know the position of one node, we can determine c (or better few candidates of c) by using (31). On the other hand, the position of one node can be evaluated by using the previous theorem (i.e. the equation (33)). The algorithm 1 describes the procedure to perform this evaluation. The algorithm computes the left hand side of equation (33), called $\theta(s_c, s)$, for every possible node candidate (s_c), which is in the interval $[0, \frac{T_S}{2}]$. The function $\theta(s_c, s)$ is independent of the second argument s when $s_c = s_n$. Indeed, $\theta(s_n, s) = -2L \forall s$. This means that the standard deviation of $\theta(s_c, s)$ respect to the second argument (s) is zero when computed in s_n (i.e. $\sigma(s_n) = 0$). When the robot sensors are affected by measurement errors, the function $\sigma(s_c)$ attains its minimum on s_n (see figures 4c, 4d, 5c, 5d and 10b).

Algorithm 1 (Returns one Node)

```

for  $s_c = 0$  to  $\frac{T_s}{2}$  do
    for  $s = 0$  to  $\frac{T_s}{2}$  do
         $\hat{s} = 2s_c - s$ 
         $\theta(s_c, s) = \beta(s) + \beta(\hat{s}) \pmod{\pi}$ 
    end for
end for
for  $s_c = 0$  to  $\frac{T_s}{2}$  do
     $\sigma(s_c) = \text{standard deviation of } \theta(s_c, s)$ 
end for
 $s_n = \arg \min_{s_c} \sigma(s_c)$ 
    
```

Once s_n is determined, equations (32) and (33) allow us to immediately evaluate the parameter L . Furthermore, as said before, equation (31) allows us to evaluate c . In both cases few possible values for these parameters are actually provided. The correct ones can be selected by combining more than one circular trajectory. On the other hand, combining at least three trajectories (with different q) is necessary also to estimate our original parameters ϕ , ψ , η , δ and ξ once the parameters ξ_q and L are evaluated for each trajectory.

Once the parameters ξ_q and L are estimated for at least three independent trajectories (i.e. corresponding to three different values of q , q_1 , q_2 and q_3), the calibration parameters ϕ , ψ , η , δ and ξ can be found by using (17), the first equation in (20) and the last equation in (22).

In particular, by having the value of ξ_q for two trajectories, it is possible to get the parameters ξ and δ by using the second equation in (17). Then, by using (17) and the first in (20) we obtain the following equation:

$$\eta_x \Psi_1^q + \eta_y = f_q$$

where $\eta_x \equiv \eta \cos \phi$, $\eta_y \equiv \eta \sin \phi$ and $f_q \equiv \xi \frac{1+q\delta}{1-q\delta}$. By using two distinct trajectories (corresponding to q_1 and q_2), we can solve the linear system

$$\begin{bmatrix} \Psi_1^{q_1} & 1 \\ \Psi_1^{q_2} & 1 \end{bmatrix} \begin{bmatrix} \eta_x \\ \eta_y \end{bmatrix} = \begin{bmatrix} f_{q_1} \\ f_{q_2} \end{bmatrix}$$

where $\Psi_1^q = \tan(\psi - L^q)$. In this way we obtain both η_x and η_y in terms of ψ . By using the third equation $\eta_x \Psi_1^{q_3} + \eta_y = f_{q_3}$ we can compute ψ .

As said in section 4.1, the information provided by the sensor data only allows us to estimate the parameters ϕ , ψ , η , δ and ξ , i.e. the calibration parameters up to a scale factor. However, by adding a supplementary metric measurement we can also estimate the original parameters ϕ , ρ , ψ , δ_R , δ_L and δ_B . Let us suppose to have the initial distance of the robot from the feature for only one among the three trajectories. Let us suppose that it is the trajectory defined by $q = q_1$. Once the parameters ϕ , ψ , η , δ and ξ are estimated as previously explained, we consider also the parameters c and k for the trajectory with $q = q_1$. By using (29) and (30) we obtain the values of A_0 and V_0 . Then, by using the first two equations in (22) we obtain the corresponding Ψ_2^q and Ψ_3^q at $s = 0$. From the last two equations in (20) we obtain the initial values γ_0 and μ_0 . On the other hand, having the initial distance D_0 allows us to obtain $\rho = \mu_0 D_0$. Once ρ is evaluated we can estimate $\delta_R = 2\rho\eta$ and then $\delta_L = \delta\delta_R$ and $\delta_B = \frac{\delta_R}{B\xi}$.

6 Performance Evaluation

We evaluate the performance of the proposed calibration strategy by carrying out both simulations and real experiments. In particular, since in the simulations the ground truth is available, we compare our strategy with a method based on an Extended Kalman Filter (*EKF*). This method uses the *EKF* to integrate the encoders data and the data provided by the camera. The matrices defining this filter can be obtained starting from the analytical expressions in (16). From now on we will refer to this calibration method with *CEKF* (Calibration based on the *EKF*).

6.1 Simulations

The dynamics of the simulated robot are described by the equations (1) and (12). The robot is equipped with encoder sensors able to provide the rotations of the right and the left wheel occurred at every time step. These encoder data are delivered at $50Hz$. Furthermore, accordingly to the model introduced in [8], all these measurements are affected by zero mean Gaussian errors independent among them. In particular, according to the error model in [8], the variance of each measurement is proportional to the value provided by the sensor. In other words, let us suppose that the true rotations of the right and left wheel occurred at a given time step are equal to $\delta\alpha_R^{true}$ and $\delta\alpha_L^{true}$. We generate the following measurements:

$$\begin{aligned}\delta\alpha^R &= N\left(\delta\alpha_R^{true}, \frac{K_R^2}{r_R}|\delta\alpha_R^{true}|\right) \\ \delta\alpha^L &= N\left(\delta\alpha_L^{true}, \frac{K_L^2}{r_L}|\delta\alpha_L^{true}|\right)\end{aligned}$$

where $N(m, \sigma^2)$ indicates the normal distribution with mean value m and variance σ^2 , r_R and r_L are respectively the nominal values of the radius of the right and left wheel, and K_R and K_L characterize the non systematic odometry error. We considered many different values for the parameters characterizing the simulated odometry system (i.e. K_R , K_L , r_R , r_L , the robot speed ν and the distance between the wheels (B) appearing in (12)). The precision of our strategy is always excellent, even when we considered values of K_R and K_L much larger (hundred times) than the values obtained through real experiments (see [8] where $K_R \simeq K_L \simeq 5 \cdot 10^{-4}m^{\frac{1}{2}}$).

In this section we provide a part of the results obtained with our simulations. In particular, we set $r \equiv r_R = r_L$, $K \equiv K_R = K_L$. In table 2 we report the parameters characterizing the robot dynamics. Observe that the chosen K is larger than the experimental values provided in [8], i.e. we are simulating encoder sensors more inaccurate and this is more challenging for the performance of our strategy.

The simulated exteroceptive sensor provides the bearings of a single feature at the origin. These data are delivered at $1Hz$. Furthermore, we assume that these bearing measurements are affected by a zero mean Gaussian error. In other words, when at a give time step the true bearing of the feature in the local frame of the sensor is β^{true} we generate the following measurement:

r	B	K	ν
$0.3m$	$0.5m$	$0.001m^{\frac{1}{2}}$	$0.05m.s^{-1}$

Table 2: The parameters characterizing the simulated odometry system.

ϕ	ρ	ψ	δ_R	δ_L	δ_B
$0.0000deg$	$0.30000m$	$90.000deg$	0.99000	1.0060	0.97000

Table 3: The true values of the calibration parameters adopted in our simulations

$$\beta = N(\beta^{true}, \sigma_\beta^2)$$

We performed many simulations by varying the value of σ_β in the range $[0, 5]deg$.

Finally, we considered many values for the calibration parameters: ϕ , ρ , ψ , δ_R , δ_L and δ_B . However, the performance of our strategy does not depend on them. For this reason, we show here a single case. Table 3 provides the values of the calibration parameters adopted in the simulations here reported.

Figure 3 reports the results obtained in the ideal case when both the odometry and the bearing sensor are noise-less (i.e. $\sigma_\beta = K = 0$). In particular, we show two cases corresponding to have the observed feature inside and outside the accomplished circular trajectory. The motion is characterized by $q = 0.8$ and the other parameters have the values previously specified. The robot trajectories and the feature are displayed in figure 3a and 3b, respectively. Figures 3c and 3e show respectively the observation function with the two nodes (red stars) and the function $\sigma(s_c)$ for the motion shown in figure 3a. s_c is the supposed position of one node. When s_c is equal to the true node position the function $\sigma(s_c)$ attains its minimum. In this case this minimum is equal to zero since it refers to an ideal case. Figures 3d and 3f refer to the case shown in figure 3b.

Figure 4 displays the results obtained by setting $\sigma_\beta = 1deg$ and the value of K specified in table 2. In this case we performed three trajectories corresponding to three different values of q : 0.9, 0 and -1 . In figure 4 we only display the results related to the case of $q = 0.9$ (figures 4a, 4c and 4e) and $q = -1$ (figures 4b, 4d and 4f). In particular, figures 4a and 4b display the observation functions with the nodes (red stars), figures 4c and 4d display the functions $\sigma(s_c)$ and figures 4e and 4f display the observation functions as observed (blue points), as estimated by our strategy alone (red points) and improved with the Levenberg Marquadt algorithm (black points) as explained in section 5. We remarked that the difference between the red and the black line is actually due to a poor estimation of the parameter k (which is obtained by only using two observations as explained in [18]). However, as explained in section 5 our strategy only needs to estimate the values of L and ξ_q for at least three trajectories and therefore the Levenberg Marquadt algorithm which only improves the estimation of k is actually unnecessary.

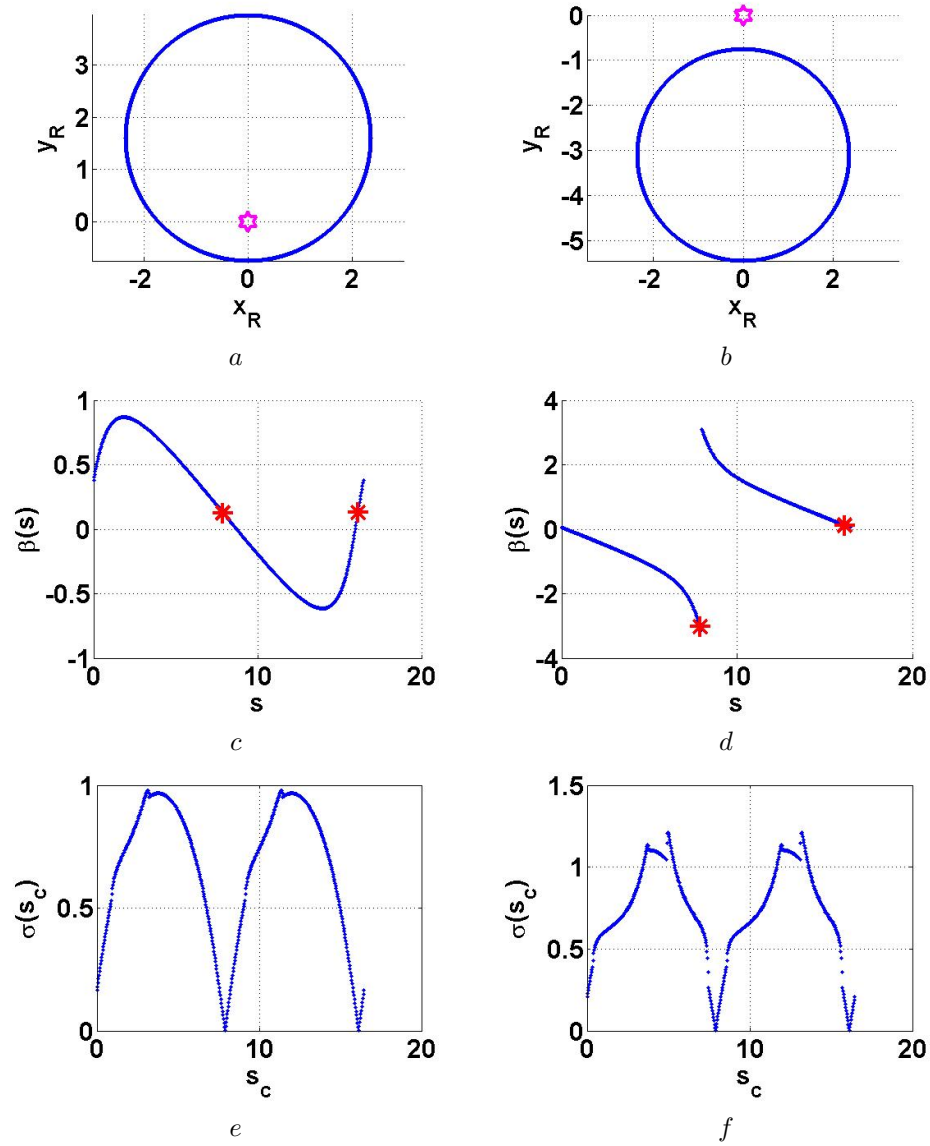


Figure 3: The phase of nodes detection in our strategy for the ideal case of perfect sensors and $q = 0.8$. *a*, *c* and *e* refer to the case when the feature is inside the accomplished trajectory while *b*, *d* and *f* when it is outside. *a* and *b* display the trajectories, *c* and *d* display the observation functions with the estimated nodes and *e* and *f* display the functions $\sigma(s_c)$.

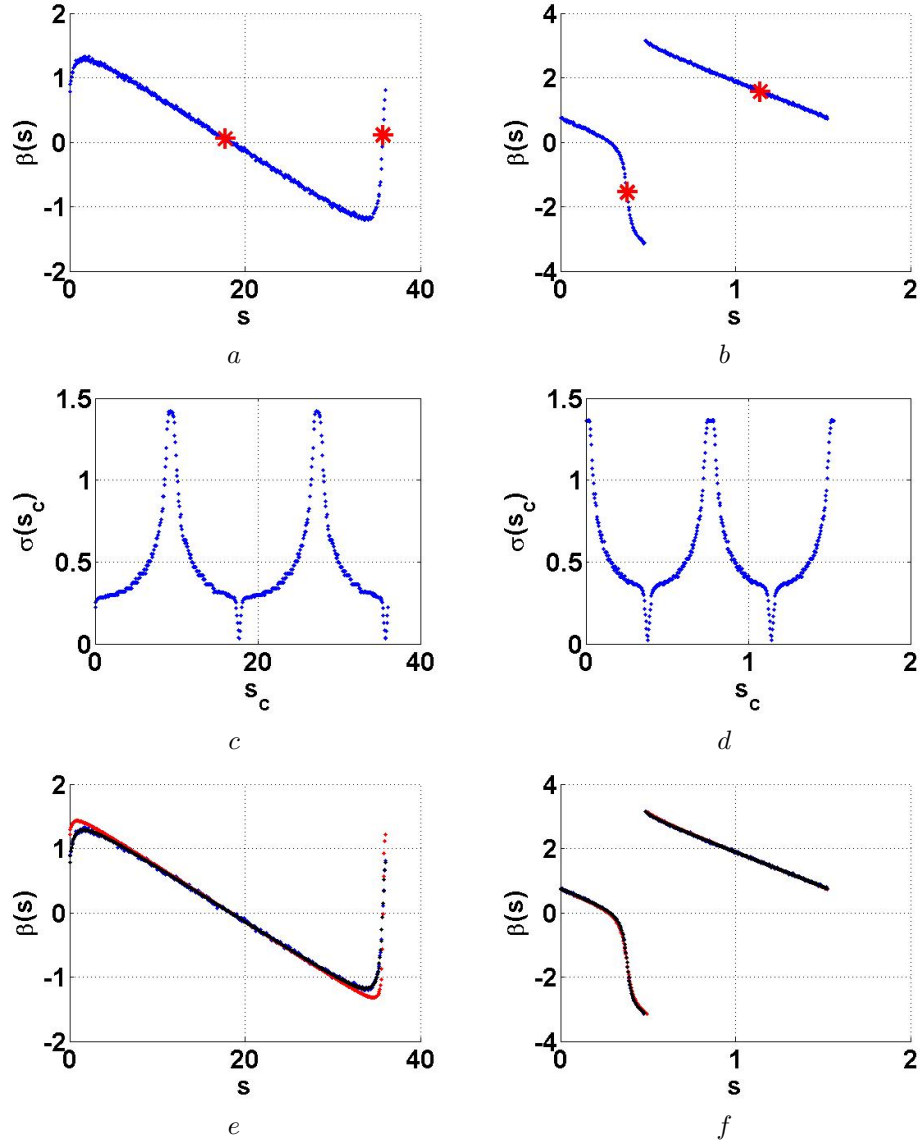


Figure 4: The estimation of the nodes and then the parameters ξ_q , L , c and k for $q = 0.9$ (*a*, *c* and *e*) and $q = -1$ (*b*, *d* and *f*). $\sigma_\beta = 1deg$ and $k = 0.001m^{\frac{1}{2}}$. *a* and *b* display the observation functions with the estimated nodes, *c* and *d* display the functions $\sigma(s_c)$ and *e* and *f* display the observation functions as observed (blue dots), as estimated by our strategy alone (red dots) and improved with the Levenberg Marquadt algorithm (black dots).

Figure 5 displays the same results shown in figure 4 but when the bearing sensor is very noisy ($\sigma_\beta = 5deg$). In this case the minimum of $\sigma(s_c)$ is significantly larger than 0 (figures 5c and 5d).

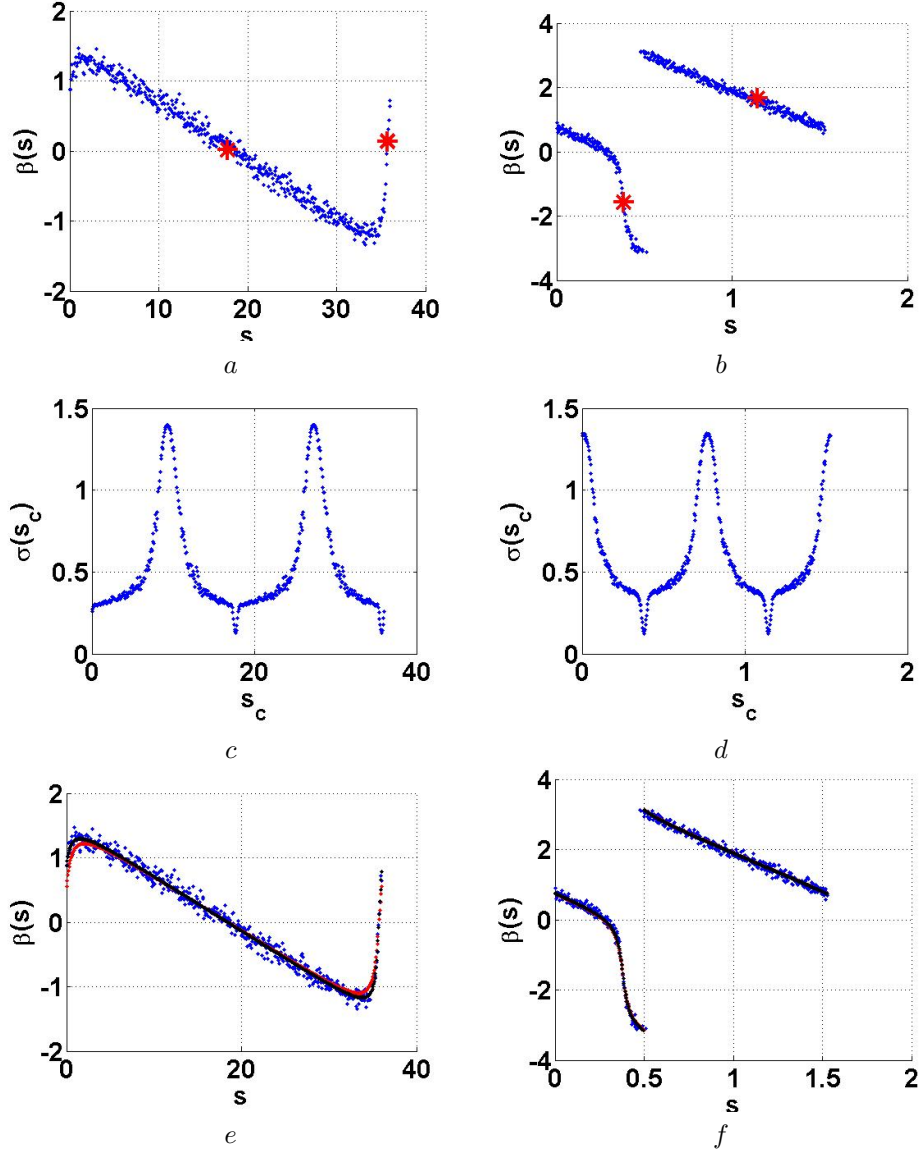


Figure 5: As in figure 4 but with a larger error on the bearing sensor ($\sigma_\beta = 5deg$).

By combining the estimated ξ_q and L for the three considered robot trajectories (i.e. with $q = 0.9, 0, -1$) we finally estimate the five parameters ϕ , ψ , η , δ and ξ . In table 4 we provide the values obtained for different errors on the bearing sensor (i.e. $\sigma_\beta = 1, 3, 5 deg$). Even with a large error on the bearing sensor ($\sigma_\beta = 5deg$) it is possible to achieve an excellent accuracy. In particular, the accuracy on the parameter δ is unbelievable (the relative error is smaller than 0.01% when $\sigma_\beta = 1deg$). We also remark that in our simulation

σ_β	ϕ (deg)	ψ (deg)	η (m^{-1})	δ	ξ (m^{-1})
True	0.00	90.0	1.6500	1.01616	2.0412
1deg	-0.08	90.05	1.6532	1.01610	2.0432
3deg	0.21	90.08	1.6454	1.01629	2.0389
5deg	0.13	89.83	1.6701	1.01607	2.0441

Table 4: The values of the calibration parameters adopted in our simulation. True values (first line) and estimated values for different σ_β .

σ_β	$\Delta\phi$ (deg)	$\Delta\psi$ (deg)	$\frac{\Delta\eta}{\eta}$	$\frac{\Delta\delta}{\delta}$	$\frac{\Delta\xi}{\xi}$
1deg	0.10	0.08	$3.2 \cdot 10^{-3}$	$5.0 \cdot 10^{-5}$	$4.5 \cdot 10^{-4}$
3deg	0.19	0.13	$5.3 \cdot 10^{-3}$	$1.2 \cdot 10^{-4}$	$8.7 \cdot 10^{-4}$
5deg	0.28	0.23	$8.5 \cdot 10^{-3}$	$1.9 \cdot 10^{-4}$	$1.3 \cdot 10^{-3}$

Table 5: The errors on the estimated parameters averaged on 100 simulations for three different σ_β .

the robot accomplishes the circular trajectory only once. It is possible to further improve the accuracy by moving the robot along more than one loop for every q and/or by considering more than three values of q . Table 4 refers to a single simulation. In order to have a more indicative result we performed 100 complete simulations obtaining 100 values for every estimated parameters. We compute the error on the estimated parameters for every simulation. In table 5 we report the mean value for these errors. It is possible to see that the relative error on the estimated parameters is particularly small (regarding δ is 0.005% when $\sigma_\beta = 1deg$). We consider this an excellent result.

6.1.1 Checking the ideal hypothesis of circular path

We investigate the impact of having a path not perfectly circular. To this goal we divide the circular path in ten thousands segments. For each one we compute the corresponding displacement for the right and the left wheel (Δs_R^c and Δs_L^c). Then, we generate the displacements of the right and left wheel (Δs_R and Δs_L) randomly with a Gaussian distribution: $\Delta s_R = N(\Delta s_R^c, (\iota \times \Delta s_R^c)^2)$ and $\Delta s_L = N(\Delta s_L^c, (\iota \times \Delta s_L^c)^2)$. We consider three cases: Model 1 where $\iota = 0$ (i.e. perfect circular trajectory), model 2 where $\iota = 0.02$ and model 3 where $\iota = 0.04$. In fig. 6 we plot the ratio $\frac{\Delta s_L}{\Delta s_R}$ vs time when the robot accomplishes a circular trajectory with $q = 0.7$. On the left it is displayed the real case obtain by using the robot AMV-1 from the BlueBotics company (see [1] for a description of the robot). On the right it is considered the simulated robot when $\iota = 0.02$. It is possible to realize that the real case satisfies the circular hypothesis better than the case when $\iota = 0.02$.

6.1.2 Comparison with CEKF

In fig. 7 we display the precision on the parameters vs the number of camera observations when the estimation is performed by the *CEKF*. In this case we set $\sigma_\beta = 0.5deg$ in order to guarantee the convergence of the *CEKF*. In

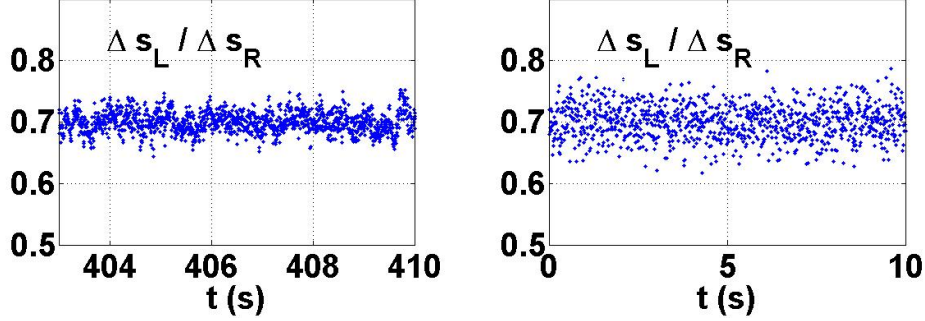


Figure 6: The ratio $\frac{\Delta s_L}{\Delta s_R}$ vs time when the robot accomplishes a circular trajectory ($q = 0.7$). On the left the result obtained with the real robot AMV-1 and on the right our simulated robot when $\iota = 0.02$.

contrast with our strategy, this filter requires to initialize the parameters. We obtained that, in order to have the convergence, the initial relative error on the parameter η must be smaller than 10%. Regarding δ and ξ the relative error must be smaller than 20%. Finally, regarding ϕ and ψ the initial error must be smaller than 10deg. From fig. 7 we remark that the convergence is very slow for the parameters ϕ , ψ and η .

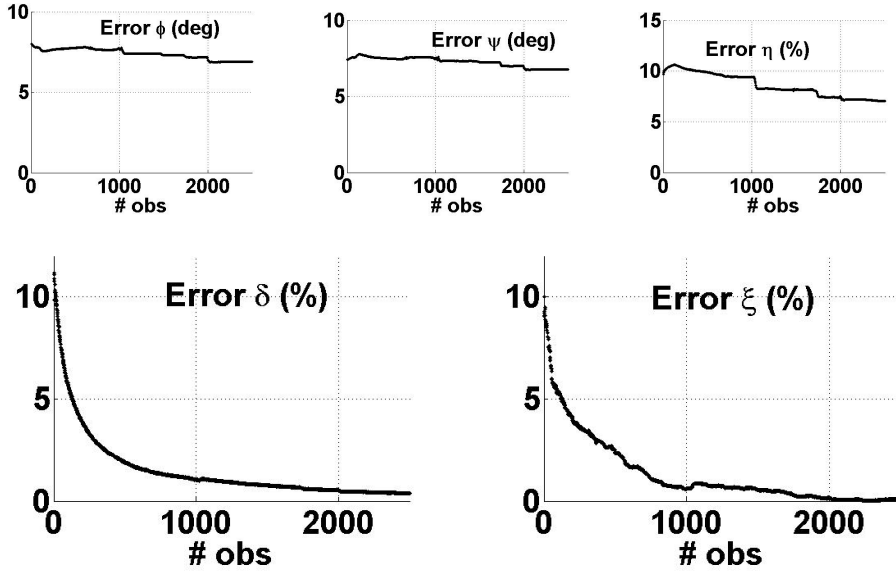


Figure 7: The precision on the parameters estimated through *CEKF* vs the number of exteroceptive observations

Table 6 compares the performance of our approach with respect to *CEKF* when the number of exteroceptive observations are 250, 500 and 1000. Even for model 3 (i.e. when $\iota = 0.04$) our method significantly outperforms *CEKF*.

<i>Mod</i>	<i>#Obs.</i>	$\Delta\phi$ <i>deg</i>	$\Delta\psi$ <i>deg</i>	$\frac{\Delta\eta}{\eta}$ %	$\frac{\Delta\delta}{\delta}$ %	$\frac{\Delta\xi}{\xi}$ %
1	250	0.06	0.05	0.5	0.02	0.07
2	250	0.5	0.3	1.2	0.04	0.12
3	250	1.1	0.4	2.7	0.07	0.14
<i>CEKF</i>	250	7.8	7.6	10	3.2	3.6
1	500	0.06	0.05	0.4	0.02	0.05
2	500	0.4	0.3	1.1	0.04	0.1
3	500	0.8	0.3	1.9	0.06	0.1
<i>CEKF</i>	500	7.7	7.5	9.8	1.9	2.5
1	1000	0.06	0.05	0.3	0.02	0.05
2	1000	0.3	0.2	0.6	0.03	0.09
3	1000	0.6	0.3	1.5	0.04	0.09
<i>CEKF</i>	1000	7.5	7.3	9.2	1.0	1.2

Table 6: The errors on the parameters averaged on 100 simulations estimated by the *CEKF* and our strategy ($\sigma_\beta = 0.5deg$).

6.2 Real Experiments

To evaluate the performance of our strategy in a real case we used the mobile robot e-puck (see [10] for a detailed description of this robot and its sensors). In our experiments we only used the camera and the odometry sensors. Actually, our strategy has been developed to calibrate an omnidirectional bearing sensor. In contrast, the available camera, has a very limited angle of view ($\simeq 38deg$). In practice, it is in general not possible to observe a single feature during the entire circular trajectory accomplished by the robot. The only situation where this is possible occurs when the feature is inside the circular trajectory (as represented in figure 3a) and close to the center. Furthermore, the camera must look towards the center of the circumference. This is the case when the angle ϕ is close to $0deg$ and ψ is close to $90deg$). Since the available camera looks ahead, we fixed in front of the robot a small mirror (see figure 8). Obviously, in these conditions our strategy cannot estimate the extrinsic calibration parameters related to the real camera. However, it estimates the parameters related to the virtual camera, i.e. the one mirrored. We remark that the goal of this experiment is not to estimate the configuration of the true camera but to validate our strategy. Therefore, we never mind whether the camera we are considering is the virtual camera.

An issue which arises when the feature is inside the trajectory is the possibility to have collisions with the feature. In order to avoid this, the circumference has to be large. In practice we could not consider trajectories with values of q smaller than 0.4.

The robot camera provides images with resolution 60×60 . Figure 9a shows the robot e-puck together with the source of light we adopted as a point feature in our experiments. Figure 9b is an image of the feature taken by the e-puck camera during our experiments. The images were provided at a frequency in the range $[0.5, 8]Hz$.

We carried out two complete experiments. In the latter we increased the radius of the right wheel by $0.062mm$ with a piece of tape. Each experi-

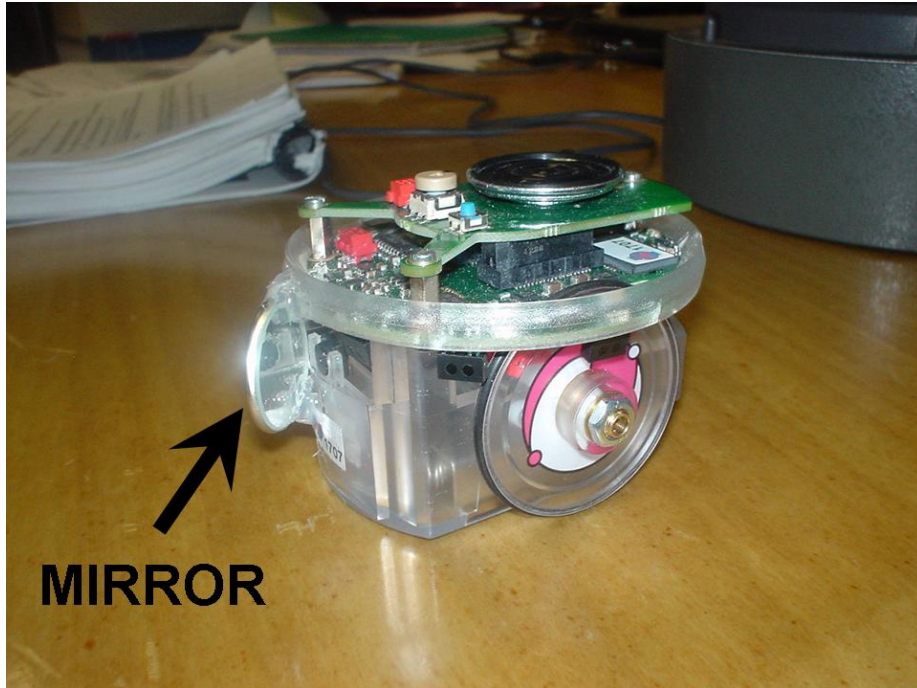


Figure 8: The robot e-puck with a small mirror in front of the camera.

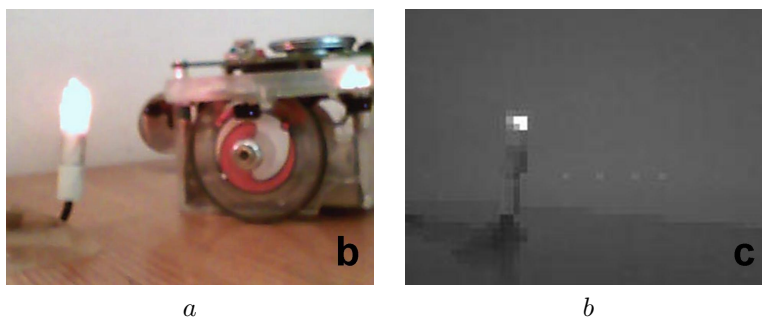


Figure 9: The robot e-puck and the source of light used as the feature (*a*) and the feature observed by the robot camera (*b*).

q	$\xi_q (m^{-1})$	$L (rad)$	$c (rad)$	$k (m^{-1})$
	No	Tape		
0.9	1.9211	1.8469	-1.4644	1.9474
0.7	5.7110	1.6382	-1.2599	6.0827
0.6	7.5937	1.5291	-1.1587	8.0819
0.4	11.4347	1.3145	-.9850	11.6104
	With	Tape		
0.9	1.9666	1.8435	-1.4703	2.0027
0.7	5.7252	1.6355	-1.2845	6.1469
0.6	7.6559	1.5279	-1.1457	8.1331
0.4	11.4092	1.3103	-0.9737	11.5967

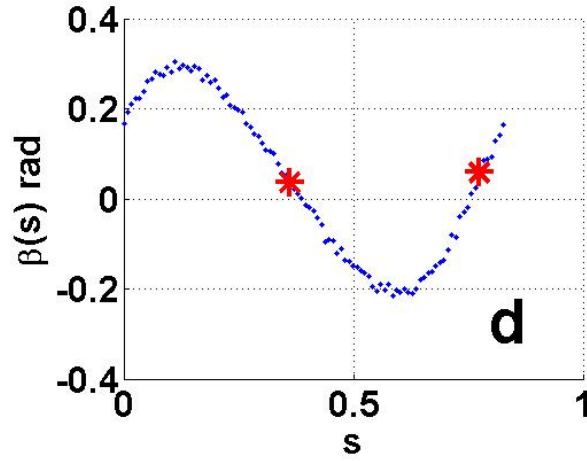
Table 7: The values of ξ_q , L , c and k obtained in our experiments for the considered trajectories.

Tape	$\phi (deg)$	$\psi (deg)$	$\eta (m^{-1})$	δ	$\xi (m^{-1})$
No	-5.80	117.18	10.21	0.9987	18.99
Yes	-5.67	116.91	10.40	0.9959	18.97

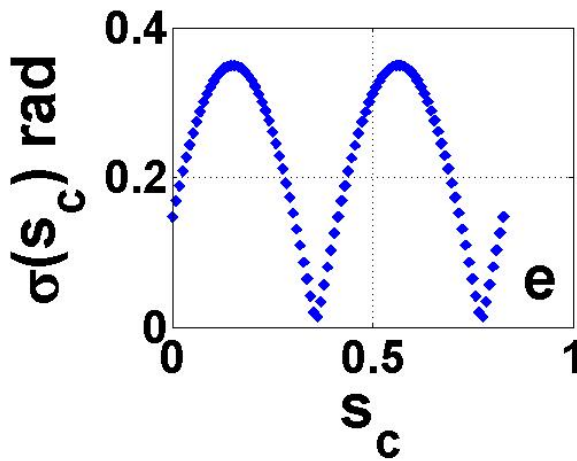
Table 8: The calibration parameters with and without tape estimated in our experiments.

ment consists of four independent trajectories with the following values of q : 0.9, 0.7, 0.6, 0.4. Regarding the estimation of the parameters ξ_q , L , c and k we show in figure 10 only the results related to the case $q = 0.6$ without tape. As for the simulations, we show the observation function with the estimated nodes (10a), the function $\sigma(s_c)$ (10b) and the observation functions as observed (blue points), as estimated by our strategy alone (red points) and improved with the Levenberg Marquadt algorithm (black points) (10c).

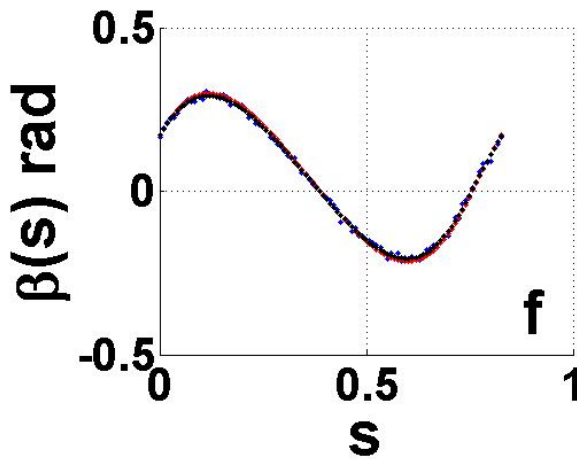
Table 7 reports the values of the parameters ξ_q , L , c and k obtained in our experiments for the different trajectories (i.e. the four considered values of q) with and without the tape on the right wheel. From these values we obtain the calibration parameters with and without tape reported in table 8. Regarding the angles ϕ and ψ , we remark that the difference between the case with tape and without tape is smaller than $0.3deg$, which is roughly the mean errors obtained in our simulations (see the second and third column of table 5). This is consistent with the fact that the tape does not affect these angle parameters. On the other hand, we remark a significant difference for the parameters η and δ . Regarding η the difference is $\simeq 2\%$ which is larger than the mean error obtained in our simulations (see the fourth column of table 5). Regarding δ the difference is $\simeq 0.3\%$ which is significantly larger than the mean error obtained in our simulations (see the fifth column of table 5). This is consistent with the increased radius of the right wheel due to the tape ($0.062mm$). In particular, since the wheel radius is $\simeq 2cm$, we obtain $\simeq 0.06mm$ for the radius change. The variation in the parameter ξ is very small and not in the expected direction. In particular, it is $\simeq 0.1\%$ which is roughly the mean error obtained in our simulations (see the last column of table 5). This parameter should be affected by the tape since it depends on δ_R . We believe that the tape also increased the



a



b



c

Figure 10: The estimation of the nodes and then the parameters ξ_q , L , c and k for $q = 0.6$ for the robot e-puck without tape. *a* displays the observation function with the estimated nodes, *b* displays the function $\sigma(s_c)$ and *c* displays the observation function as observed (blue points), as estimated by our strategy alone (red points) and improved with the Levenberg Marquadt algorithm (black points).

effective distance between the wheels (i.e. the parameter δ_B) making $\xi = \frac{1}{B} \frac{\delta_R}{\delta_B}$ unaffected by the tape.

7 Conclusions

In this paper we considered the problem of estimation in autonomous navigation from a theoretical perspective. In particular, the investigation regarded problems where the information provided by the sensor data is not sufficient to carry out the state estimation (i.e. the state is not observable). In order to properly exploit the information in the sensor data, it is necessary to separate the observable part of the system from the rest. In this paper we used the concept of continuous symmetry to achieve this goal. We then illustrated this concept by investigating a fundamental calibration problem in autonomous navigation. In particular, the decomposition for our calibration problem was based on the solutions of two partial differential equations which express the continuous symmetries of the considered system.

The paper introduced two original distinct contributions:

- The introduction, in the frame work of autonomous navigation, of the concept of continuous symmetry and its application in order to locally separate the observable part from the rest of the system.
- A simple strategy to robustly, efficiently and accurately estimate the parameters describing both the extrinsic bearing sensor calibration and the odometry calibration.

The performance of the proposed strategy was carefully evaluated by carrying out both simulations and real experiments with the mobile robot e-puck. In both cases, we found excellent results in terms of precision, robustness and facility of implementation.

To the best of our knowledge, the concept of continuous symmetry has never been exploited in the framework of autonomous navigation. We believe that it is a very powerful tool to face many estimation problems in the frame-work of mobile robotics and this paper is its first very successful application. To this regard, future works will focus on the application of this concept in order to solve other estimation problems. In particular, in the framework of self calibration we are currently considering the case of range sensors and other kind of features. Furthermore, we want to extend the calibration to $3D$. Finally, we want to consider other estimation problems in the framework of cooperative localization and cooperative SLAM where the concept of continuous symmetry could have a big impact.

8 Appendix

A: Observability for the system defined by equation (16)

Let us refer to the system whose dynamics and observation are defined in (16). Accordingly to the rank criterion, we have to provide five Lie derivatives whose gradients span the entire configuration space. Let us consider the matrix whose lines are the gradients of the Lie derivatives $L^0\beta$, $L_{f_1}^1\beta$, $L_{f_2}^1\beta$, $L_{f_1f_1}^2\beta$, $L_{f_1f_2}^2\beta$, $L_{f_2f_1}^2\beta$ and $L_{f_2f_2}^2\beta$, where f_1 and f_2 are defined in (??). The determinant of this matrix is: $-16\delta^4\mu^5\eta^3\xi^5\cos(\gamma-\phi)(\mu\cos\phi-\cos(\gamma-\phi))/(\mu^2+2\mu\cos\gamma+1)^5$ which is in general different from 0.

References

- [1] <http://www.bluebotics.com/automation/AMV-1/>
- [2] G. Antonelli and S. Chiaverini, Linear estimation of the physical odometric parameters for differential-drive mobile robots, *Autonomous Robot*, Vol 23, pages 59-68
- [3] Bicchi A., Praticchizzo D., Marigo A. and Balestrino A., On the Observability of Mobile Vehicles Localization, *IEEE Mediterranean Conference on Control and Systems*, 1998
- [4] Bonnifait P. and Garcia G., Design and Experimental Validation of an Odometric and Goniometric Localization System for Outdoor Robot Vehicles, *IEEE Transaction On Robotics and Automation*, Vol 14, No 4, August 1998
- [5] Borenstein J., Feng L., "Measurement and correction of systematic odometry errors in mobile robots," *IEEE Transactions on Robotics and Automation*, vol. 12, pp. 869–880, 1996.
- [6] Brogan, William L. *Modern Control Theory*, 3rd ed. Englewood Cliffs, NJ: Prentice Hall, 1991
- [7] X. Brun and F. Goulette, Modeling and calibration of coupled fisheye CCD camera and laser range scanner for outdoor environment reconstruction, in *Proceedings of the International Conference on 3D Digital Imaging and Modeling*, Montreal, QC, Canada, Aug. 2123, 2007, pp. 320327.
- [8] Chong K.S., Kleeman L., "Accurate Odometry and Error Modelling for a Mobile Robot," *International Conference on Robotics and Automation*, vol. 4, pp. 2783–2788, 1997.
- [9] Doh, N. L., Choset, H. and Chung, W. K., Relative localization using path odometry information, *Autonomous Robots*, Vol 21, pages 143-154
- [10] <http://www.e-puck.org/>
- [11] Hermann R. and Krener A.J., 1977, Nonlinear Controllability and Observability, *IEEE Transaction On Automatic Control*, AC-22(5): 728-740
- [12] G.P. Huang, A.I. Mourikis, and S.I. Roumeliotis, "Analysis and improvement of the consistency of extended Kalman filter based Slam", In *Proceedings of the 2008 IEEE International Conference on Robotics and Automation (ICRA)*, pages 473479, May 2008.
- [13] Isidori A., *Nonlinear Control Systems*, 3rd ed., Springer Verlag, 1995.
- [14] Kosut R.L., Arbel A. and Kessler K.M., Optimal Sensor System Design for State Reconstruction, *IEEE Transaction On Automatic Control*, Vol 27, No 1, February 1982
- [15] Lee K. W., Wijesoma W. S. and Guzman J.I., On the Observability and observability analysis of SLAM. In *Proceedings of IEEE International Conference on Intelligent Robots and Systems*, Benjing, China, October 2006.

-
- [16] Lorussi F, Marigo A. and Bicchi A., Optimal exploratory paths for a mobile rover, IEEE International Conference on Robotics and Automation (ICRA), 2001, Vol 2, Pages:2078 - 2083
- [17] Martinelli A, "The odometry error of a mobile robot with a synchronous drive system", *IEEE Trans. on Robotics and Automation* Vol 18, NO. 3 June 2002, pp 399–405
- [18] Martinelli A, Using the Distribution Theory to Simultaneously Calibrate the Sensors of a Mobile Robot, Internal Research Report, INRIA, <http://hal.inria.fr/docs/00/35/30/79/PDF/RR-6796.pdf>
- [19] A. Martinelli and R. Siegwart, Observability Analysis for Mobile Robot Localization, International Conference on Intelligent Robots and Systems, Edmonton, Canada, August 2005.
- [20] A. Martinelli, D. Scaramuzza and R. Siegwart, Automatic Self-Calibration of a Vision System during Robot Motion, International Conference on Robotics and Automation, Orlando, Florida, April 2006.
- [21] A. Martinelli and R. Siegwart, Observability Properties and Optimal Trajectories for On-line Odometry Self-Calibration. In Proceedings of IEEE International Conference on Decision and Control, San Diego, California, December 2006.
- [22] A. Martinelli, N. Tomatis and R. Siegwart, Simultaneous Localization and Odometry Self Calibration for Mobile Robots, *Autonomous Robot*, Vol 22 Issue 1, January 2007, pages 75-85
- [23] A. Martinelli, Local Decomposition and Observability Properties for Automatic Calibration in Mobile Robotics, International Conference on Robotics and Automation, Kobe, Japan, May 2009.
- [24] Martinelli A, Using the Distribution Theory to Simultaneously Calibrate the Sensors of a Mobile Robot, to be presented at RSS 2009, Seattle, June 2009.
- [25] F. M. Mirzaei and S. I. Roumeliotis, A Kalman filter-based algorithm for IMU-camera calibration: Observability analysis and performance evaluation, *IEEE Transactions on Robotics*, 2008, Vol. 24, No. 5, October 2008, pages 1143-1156
- [26] Park F. C. and B. J. Martin, Robot Sensor Calibration: Solving $AX=XB$ on the Euclidean Group, *IEEE Trans. on Rob. and Aut.*, Vol 10, No 5 Oct 1994.
- [27] S.I. Roumeliotis and G.A. Bekey, 2002, Distributed Multirobot Localization, *IEEE Transaction On Robotics and Automation* Vol 18, No.5, October 2002
- [28] Roy N., and Thrun S., Online Self-calibration for Mobile Robots, proceedings of the 1999 IEEE International Conference on Robotics and Automation, 19 May 1999 Detroit, Michigan, pp. 2292-2297.

-
- [29] Shiu Y. C. and S. Ahmad, Calibration of Wrist-Mounted Robotic Sensors by Solving Homogeneous Transform Equations of the Form $AX=XB$, *IEEE Trans on Rob. and Aut.* Vol 5 No 1 Feb 1989
 - [30] H.J. von der Hardt, R. Husson, D. Wolf, An Automatic Calibration Method for a Multisensor System: Application to a Mobile Robot Localization System, *International Conference on Robotics and Automation*, Leuven, Belgium, May 1998.
 - [31] S. Wasielewski and O. Strauss, Calibration of a multi-sensor system laser rangefinder/camera, in *Proceedings of the Intelligent Vehicles Symposium*, Detroit, MI, Sept. 25-26, 1995, pp. 472-477.
 - [32] Q. Zhang and R. Pless, Extrinsic calibration of a camera and laser range finder (improves camera calibration), in *Proceedings of the IEEE/RSJ International Conference on Intelligent Robots and Systems*, Sendai, Japan, Sept. 28-Oct. 2, 2004, pp. 2301-2306.

Contents

1	Introduction	3
1.1	Related Works on Sensor Calibration in Mobile Robotics	4
1.2	Related Works on Observability Analysis in Mobile Robotics	5
1.3	Paper Contributions and Paper Structure	6
2	A Simple Example of Localization	6
3	Continuous Symmetries and Observability Properties	8
3.1	Observability Rank Criterion	9
3.2	Local Decomposition	9
3.3	Continuous Symmetries	10
4	The Problem of Simultaneous Odometry and Bearing Sensor Calibration	12
4.1	The Considered System	12
4.2	Deriving the WLO Quantities for Circular Trajectories	14
4.3	Analytical Properties of the Observation Function	16
5	The Strategy to Estimate the System Parameters	18
6	Performance Evaluation	20
6.1	Simulations	20
6.1.1	Checking the ideal hypothesis of circular path	25
6.1.2	Comparison with CEKF	25
6.2	Real Experiments	27
7	Conclusions	31
8	Appendix	32



Centre de recherche INRIA Grenoble – Rhône-Alpes
655, avenue de l'Europe - 38334 Montbonnot Saint-Ismier (France)

Centre de recherche INRIA Bordeaux – Sud Ouest : Domaine Universitaire - 351, cours de la Libération - 33405 Talence Cedex
Centre de recherche INRIA Lille – Nord Europe : Parc Scientifique de la Haute Borne - 40, avenue Halley - 59650 Villeneuve d'Ascq
Centre de recherche INRIA Nancy – Grand Est : LORIA, Technopôle de Nancy-Brabois - Campus scientifique
615, rue du Jardin Botanique - BP 101 - 54602 Villers-lès-Nancy Cedex
Centre de recherche INRIA Paris – Rocquencourt : Domaine de Voluceau - Rocquencourt - BP 105 - 78153 Le Chesnay Cedex
Centre de recherche INRIA Rennes – Bretagne Atlantique : IRISA, Campus universitaire de Beaulieu - 35042 Rennes Cedex
Centre de recherche INRIA Saclay – Île-de-France : Parc Orsay Université - ZAC des Vignes : 4, rue Jacques Monod - 91893 Orsay Cedex
Centre de recherche INRIA Sophia Antipolis – Méditerranée : 2004, route des Lucioles - BP 93 - 06902 Sophia Antipolis Cedex

Éditeur
INRIA - Domaine de Voluceau - Rocquencourt, BP 105 - 78153 Le Chesnay Cedex (France)
<http://www.inria.fr>
ISSN 0249-6399